Acta Mechanica Sinica (2014) 30(2):214–222
DOI 10.1007/s10409-013-0097-z

RESEARCH PAPER

Stability analysis of a thin-walled cylinder in turning operation using the semi-discretization method

Arnab Chanda · Achim Fischer · Peter Eberhard · Santosha Kumar Dwivedy

Received: 19 July 2013 / Accepted: 7 November 2013

Abstract In this work, the stability of a flexible thin cylindrical workpiece in turning is analyzed. A process model is derived based on a finite element representation of the workpiece flexibility and a nonlinear cutting force law. Repeated cutting of the same surface due to overlapping cuts is modeled with the help of a time delay. The stability of the so obtained system of periodic delay differential equations is then determined using an approximation as a time-discrete system and Floquet theory. The time-discrete system is obtained using the semi-discretization method. The method is implemented to analyze the stability of two different workpiece models of different thicknesses for different tool positions with respect to the jaw end. It is shown that the stability chart depends on the tool position as well as on the thickness.

Keywords Machine tools · Stability · Chatter

1 Introduction

In manufacturing science, chatter is a well known subject of research. The term chatter is used to refer to self-excited vibrations that deteriorate the precision of the machining operation. Generally, chatter leads to large amplitude vibrations which cause poor surface finish, increase tool wear, minimize the tool life and ultimately damage the machine tool. At the beginning of the nineteenth century, Taylor [1], identified the chatter phenomenon during machining process as greatly limiting the productivity.

From that till today, Arnold [2], Tobias [3], Merrit [4], Tlusty and Polacek [5] and many others have proposed models to explain the chatter. Clancy and Shin [6] have determined the stability boundaries for three dimensional face turning processes considering the frequency domain chatter model with process damping. Ozlu and Budak [7] have proposed an analytical model for the stability limit prediction of the multi-dimensional model with three dimensional geometry of the process to observe the effect of the tool tip nose radius and tool angle on the stability limit. Later, Ozlu and Budak [8] made a comparative study between the one-dimensional and multi-dimensional stability model in turning operations. Zhongqun and Qing [9] demonstrated a time domain simulation to study the dynamics of end milling considering the regenerative chatter using a special chatter detection criterion applying synthetically the simulated signals. Srinivas and Kotaiah [10] analyzed the linear stability in turning process using the non-linear force feed dynamic model by considering the three dimensional cutting tool geometry. Mehdi et al. [11, 12] investigated the chatter vibration problem for turning of a thin walled cylinder using FEM.

Very often, it is considered that the cutting tool is flexible and the workpiece is rigid. In this work, the workpiece model is thin-walled and thus elastically deformable. Furthermore, with the workpiece rotation, the relative position of the tool with respect to the workpiece changes with time. This makes the input and output behavior of the system time variant and periodic. Consecutive cuts on the same surface generate a time delay system. All these lead to a time-variant periodic delayed system.

Stability analysis of this time variant periodic system of delay differential equations is a difficult task that can only be solved using time-domain simulations or approximating methods. Two approximating methods have been suggested in recent time that receive a lot of interest. Bayly and Davis [13] analyzed the stability of interrupted milling and other cutting operations using the temporal finite element analysis (TFEA) method. Insperger and Stépán [14] have introduced a special kind of discretization technique, the Semi-Discretization Method, where only the past is discretized to analyze the stability. The stability of the system is determined with the help of the eigenvalues of the monodromy

A. Chanda · A. Fischer · P. Eberhard (✉) · S. K. Dwivedy
Institute of Engineering and Computational Mechanics,
University of Stuttgart, Stuttgart 70569, Germany
e-mail: peter.eberhard@itm.uni-stuttgart.de

matrix of the approximated discrete system. Insperger and Stépán [15] further established a modified version of the semi-discretization method especially for periodic systems with single discrete time delay. The delayed term is approximated as a weighted linear combination of two neighboring delayed discrete state values. Henninger and Eberhard [16] proposed different measures to increase the computational efficiency of the semi-discretization method.

2 System modeling

Figure 1 shows a photograph of the inside turning process of a thin walled cylinder clamped at one end by a three jaw chuck. In contrast to most of the machine tool chatter models found in literature, the workpiece flexibility can not be neglected here. Hence the tool is considered to be rigid and the workpiece modeled as a flexible body undergoing deformation.

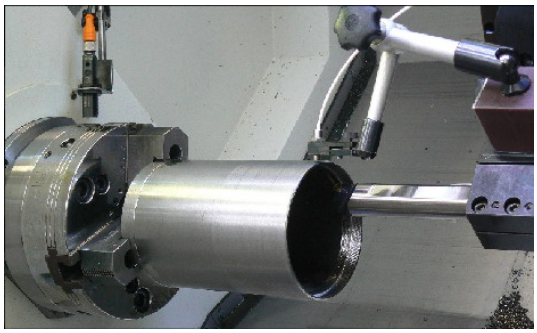

Fig. 1 Cylindrical workpiece on lathe

To study the dynamic behavior and the deformation of the flexible workpiece model, the finite element analysis has been carried out using the commercial software ANSYS. As the high number of nodal degrees of freedom makes it difficult to analyze the dynamics of a finite-degree of freedom workpiece model in nodal coordinates, model order reduction using a limited number of vibration modes is used to reduce the system dimension and uncouple the equations from each other. The workpiece model is transformed from the nodal coordinate system to the modal coordinate system using the modal matrix which is obtained by solving the generalized eigenvalue problem of the system for free vibration.

Thus, after performing the necessary operations, the equation of motion of the system can be written in modal form by the second order differential equation. But, the implemented stability analysis procedure needs a system in state space form. Therefore, the second order equation of motion of the workpiece model is constructed in state space form, see Ref. [17]

$$\dot{\boldsymbol{q}} = \boldsymbol{A} \cdot \boldsymbol{q} + \boldsymbol{B}(t) \cdot \boldsymbol{f}(t), \tag{1}$$

$$\tilde{\boldsymbol{q}} = \boldsymbol{C}(t) \cdot \boldsymbol{q}. \tag{2}$$

In Eqs. (1) and (2), $\boldsymbol{q}(t) \in \mathbb{R}^{n_\mathrm{m}\times 1}$ is the displacement vector in modal coordinates, $\boldsymbol{A} \in \mathbb{R}^{2n_\mathrm{m}\times 2n_\mathrm{m}}$ is called the system matrix, $\boldsymbol{f}(t) \in \mathbb{R}^{n_\mathrm{i}\times 1}$ is the input force vector, $\boldsymbol{B}(t) \in \mathbb{R}^{2n_\mathrm{m}\times n_\mathrm{i}}$ the input matrix and $\boldsymbol{C}(t) \in \mathbb{R}^{n_\mathrm{o}\times 2n_\mathrm{m}}$ the output matrix. Here, n_m is the reduced number of modes, n_i is the dimension of the external force, n_o is the dimension of the output displacement vector. Note that the input and output matrices are time-varying due to workpiece rotation and tool feed.

In the present stability analysis, three dimensional oblique cutting is considered. The tool cutting force consists of three components: cutting force F_c, feed force F_f and thrust force F_t as illustrated in Fig. 2. Therefore, the three dimensional cutting force $\boldsymbol{f}(t)$ at the contact point of the tool tip and the workpiece surface in Eq. (1) can be written as

$$\boldsymbol{f}(t) = [F_\mathrm{t}(t) \;\; F_\mathrm{c}(t) \;\; F_\mathrm{f}(t)]^\mathrm{T}. \tag{3}$$

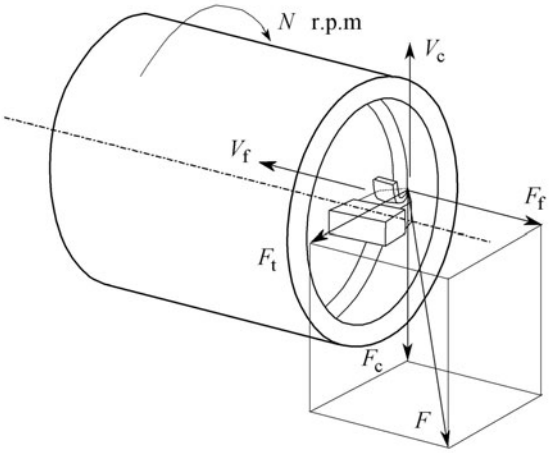

Fig. 2 Three dimensional cutting forces in turning

The material removal operation is a complex process where the cutting forces are mainly affected by the chip and tool geometry and workpiece material. According to most cutting force laws, the forces are modeled as functions of chip thickness and chip width using specific force components, see Ozlu and Budak [7], Srinivas and Kotaiha [10]. For unit cross sectional area of the chip at given workpiece materials and process conditions, the values of these specific force components can be determined here with the help of the experimental results of König et al. [18]. The three cutting force components can be written as

$$F_\mathrm{c}(t) = K_\mathrm{c} b(t) h(t) \left(\frac{h_\mathrm{ref}}{h(t)}\right)^{m_y} = K_\mathrm{c} b(t) h_\mathrm{ref}^{m_y} h(t)^{(1-m_y)}, \tag{4}$$

$$F_\mathrm{f}(t) = K_\mathrm{f} b(t) h_\mathrm{ref}^{m_z} h(t)^{(1-m_z)}, \tag{5}$$

$$F_\mathrm{t}(t) = K_\mathrm{t} b(t) h_\mathrm{ref}^{m_x} h(t)^{(1-m_x)}, \tag{6}$$

where $h(t)$ is the chip thickness, $b(t)$ is the chip width, h_ref is the basis of chip thickness as taken in the experiment [18]. The parameter K_c is the specific cutting force, K_f the spe-

cific feed force and K_t the specific thrust force. The numerical values for the coefficients are taken from literature, e.g., from Ref. [19].

To analyze the stability, a small variation of chip width and thickness around their nominal values b_0 and h_0 has been considered. The expression of the parametric cutting force can then be obtained using the Taylor series expansion

$$F_c(t) = F_{c,0} + \Delta F_c(t) = F_{c,0} + \frac{\partial \Delta F_c}{\partial b}\Delta b + \frac{\partial \Delta F_c}{\partial h}\Delta h. \quad (7)$$

Here, only the linear terms are considered. As the nominal cutting force $F_{c,0}$ does not contribute to the dynamic behavior, we consider only the variation of the cutting force from its nominal value

$$\Delta F_c(t) = K_c h_{ref}^{m_y}[h_0^{(1-m_y)}\Delta b + (1-m_y)b_0 h_0^{-m_y}\Delta h]. \quad (8)$$

In similar way, the expression for $\Delta F_t(t)$ and $\Delta F_f(t)$ can be evaluated. In Fig. 3, it is shown that the tool is moving along the z-direction with feed f towards the jaw. The depth of cut a_p is defined along the x-direction, κ is the tool cutting edge angle.

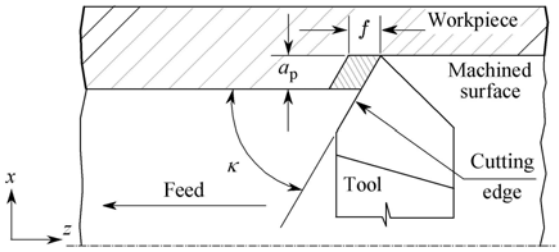

Fig. 3 Schematic view of metal cutting of the hollow cylinder

Using Fig. 4, the instantaneous chip thickness and width can be expressed by the workpiece deformation in z- and x-direction as

$$h(t) = h_0 - \Delta x\cos\kappa + \Delta z\sin\kappa, \quad (9)$$

$$b(t) = b_0 - \frac{\Delta x}{\sin\kappa}. \quad (10)$$

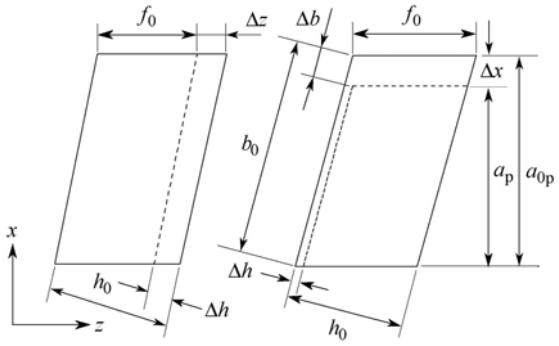

Fig. 4 Chip size variation due to deformation

Here, the solid line shows the deformed position of the workpiece surface and the dotted line shows the initial position of the workpiece surface, Δx and Δz are the variations of the depth of cut a_{0p} and longitudinal feed f_0 of the tool. The expressions in Eqs. (9) and (10) clearly depict that workpiece deformation in tool feed direction varies the nominal chip thickness h, whereas workpiece deformation in depth of cut direction contributes to both the chip thickness h and chip width b.

Using Eqs. (9) and (10), the expressions for the variation of cutting force components are obtained from Eq. (8) and expressions for $\Delta F_t(t)$ and $\Delta F_f(t)$ in terms of directional specific cutting forces, feed and depth of cut

$$\Delta \boldsymbol{f} = \boldsymbol{G}\cdot[-\Delta x\ \ \Delta z]^T, \quad (11)$$

where

$$\Delta \boldsymbol{f} = [\Delta F_t\ \ \Delta F_c\ \ \Delta F_f]^T, \quad \boldsymbol{G} = \begin{pmatrix} K_{tx} & K_{tz} \\ K_{cx} & K_{cz} \\ K_{fx} & K_{fz} \end{pmatrix},$$

and the coefficients of $\boldsymbol{G}$ read

$$K_{cx} = K_c h_{ref}^{m_y}\left[\frac{h_0^{(1-m_y)}}{\sin\kappa} + (1-m_y)b_0 h_0^{-m_y}\cos\kappa\right],$$

$$K_{cz} = K_c h_{ref}^{m_y}[(1-m_y)b_0 h_0^{-m_y}\sin\kappa],$$

$$K_{fx} = K_f h_{ref}^{m_z}\left[\frac{h_0^{(1-m_z)}}{\sin\kappa} + (1-m_z)b_0 h_0^{-m_z}\cos\kappa\right],$$

$$K_{fz} = K_f h_{ref}^{m_z}\left[(1-m_z)b_0 h_0^{-m_z}\sin\kappa\right],$$

$$K_{tx} = K_t h_{ref}^{m_x}\left[\frac{h_0^{(1-m_x)}}{\sin\kappa} + (1-m_x)b_0 h_0^{-m_x}\cos\kappa\right],$$

$$K_{tz} = K_t h_{ref}^{m_x}\left[(1-m_x)b_0 h_0^{-m_x}\sin\kappa\right].$$

Due to the deformation of the workpiece, a wavy surface is cut. Because of the overlapping of successive cuts, this wavy surface will cause a variation of tool feed and depth of cut after one rotation. The expression for the actual chip geometry depends thus not only on the current movements of tool and workpiece, but also on the past movements of the workpiece, see Fig. 5.

In Fig. 5, the thick line shows the surface created by the previous cut, a_{0p} is the nominal depth of cut and the workpiece displacement at the tool tip contact point along the positive x-direction is $x(t)$. The variation of tool depth of cut along the x-direction is then $\Delta x(t) = a_p(t) - a_{0p}$. Further, the actual depth of cut becomes

$$a_p(t) = a_{0p} - x(t) + \mu x(t-\tau) \Rightarrow \Delta x = \mu x(t-\tau) - x(t). \quad (12)$$

The time delay τ in $x(t-\tau)$ depends on the rotational speed N of the cylindrical workpiece. The factor μ is used to describe the overlapping of successive cuts. We consider here an overlap of $\mu = 1$. In the considered inside turning

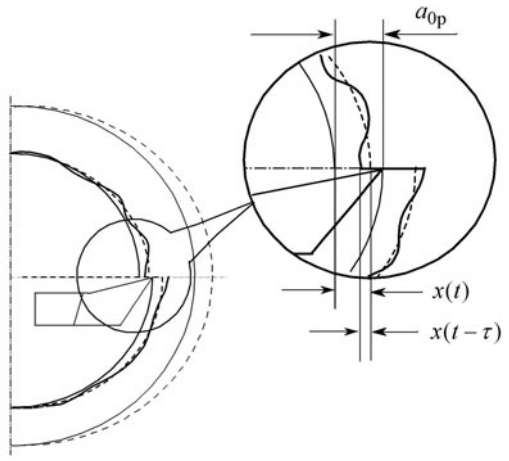

Fig. 5 Depth of cut variation due to deformation

operation, the actual overlap is smaller than 1 due to the tool feed. However, as the tool moves only a small fraction of the blade length during one rotation, the actual overlapping is close to one. Taking $\mu = 1$ represents a worst-case scenario.

In a similar way, the tool feed variation is $\Delta z = f(t) - f_0(t)$, with the actual tool feed

$$f(t) = f_0 + z(t) - z(t-\tau), \tag{13}$$

$$\Rightarrow \quad \Delta z = f(t) - f_0(t) = z(t) - z(t-\tau). \tag{14}$$

Inserting Δx and Δz in Eq. (11) and then replacing the displacement $(x(t)\ z(t))^{\mathrm{T}}$ at the contact point with help of the output displacement matrix from Eq. (2), the cutting force variation can be expressed as

$$\Delta \boldsymbol{f}(t) = \boldsymbol{G} \cdot \begin{pmatrix} (x(t) - x(t-\tau)) \\ (z(t) - z(t-\tau)) \end{pmatrix}$$
$$= \boldsymbol{G} \cdot \boldsymbol{C}(t) \cdot (\boldsymbol{q} - \boldsymbol{q}(t-\tau)). \tag{15}$$

As the tool contact point changes with time, the output matrix $\boldsymbol{C}$ is also time-variant. Expressing the variation of cutting force $\Delta \boldsymbol{f}(t)$ in terms of $\boldsymbol{G}$, $\boldsymbol{C}(t)$ and the present and past output displacement vectors, Eqs. (1) and (2) give the model of the considered turning operation in state space form

$$\dot{\boldsymbol{q}} = \tilde{\boldsymbol{A}}(t) \cdot \boldsymbol{q} - \tilde{\boldsymbol{B}}(t) \cdot \boldsymbol{q}(t-\tau), \tag{16}$$

with time varying coefficient matrices $\tilde{\boldsymbol{A}}(t)$ and $\tilde{\boldsymbol{B}}(t)$, where $\tilde{\boldsymbol{A}}(t) = \boldsymbol{A} + \boldsymbol{B}(t) \cdot \boldsymbol{G} \cdot \boldsymbol{C}(t)$ and $\tilde{\boldsymbol{B}}(t) = \boldsymbol{B}(t) \cdot \boldsymbol{G} \cdot \boldsymbol{C}(t)$. The system (16) is time-variant because of the changing input and output behaviour due to workpiece rotation and tool feed. It is to be noted that, as the tool feed is comparably small, it can be neglected. Neglecting the tool feed leads to a periodic system, i.e., $\tilde{\boldsymbol{A}}(t) = \tilde{\boldsymbol{A}}(t+T)$ and $\tilde{\boldsymbol{B}}(t) = \tilde{\boldsymbol{B}}(t+T)$. Periodicity is an important prerequisite for the stability analysis procedure presented in the following section. The interesting part of the system equation is, that it includes the effect of both tool feed and depth of cut variation. It also incorporates the three dimensional cutting force.

3 Stability analysis using the semi-discretization method

Consecutive cuts on the same surface, modeled in Eq. (16) as an interaction of the time-delay of the system and the system dynamics, can lead to instability. The equations of motion of the considered turning process form a system of periodic delay differential equations. Analysis of its stability is a difficult task that has received and still receives a lot of interest in the scientific community. Although Floquet-Theory, see Hale and Lunel [22], can be applied to systems with time delay, practical application is not straight-forward. One reason is that the introduction of the time delay in the time periodic dynamical system causes the phase space to grow from finite dimension to infinite dimension, which leads to an infinite dimensional monodromy matrix.

To solve this problem, the semi-discretization method, proposed by Insperger and Stépán [14], is followed to analyze the time-periodic DDE with discrete delay. The infinite dimensional system is hereby approximated by a finite dimensional one by finite discretization of the time coordinates. Here, this method is briefly described.

The first step is to divide the delay time part into small time intervals $[t_i, t_{i+1}]$ of length Δt, as shown in Fig. 6. The number of time intervals k is chosen such that $T = k\Delta t$, k can be considered as an approximation parameter regarding the periodicity of the system. An integer m is introduced for the approximation of the time delay term, i.e., $\tau = m\Delta t$. It is to be noted that the periodicity of the system and the time delay are here equal, i.e., $T = \tau$. Thus, the integers k and m will also be equal.

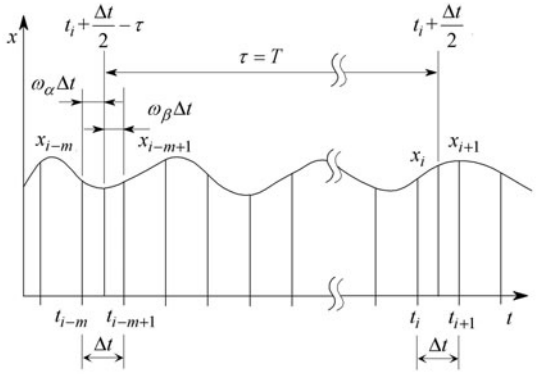

Fig. 6 Approximation of the delay term by discrete time steps

If the notation $x(t_j) = x_j$ is used, then for the i-th interval, the delay equation (16) can be approximated as

$$\dot{\boldsymbol{q}}(t) = \tilde{\boldsymbol{A}}_i \cdot \boldsymbol{q}(t) - \tilde{\boldsymbol{B}}_i \cdot (\omega_\alpha \boldsymbol{q}_{i-m+1} + \omega_\beta \boldsymbol{q}_{i-m}), \tag{17}$$

where the time dependent matrices $\tilde{\boldsymbol{A}}_i(t)$ and $\tilde{\boldsymbol{B}}_i(t)$ are approximated by their mean values in the interval $[t_i, t_{i+1}]$. As in Ref. [15], the delay term $\boldsymbol{q}(t-\tau)$ is approximated as a weighted linear sum of the discrete states $\boldsymbol{q}_{i-m}$ and $\boldsymbol{q}_{i-m+1}$

where ω_α and ω_β are the weighting factors for constant interpolation.

The state $\boldsymbol{q}_{i+1}$ at the end of the interval i is obtained by integrating the piece-wise autonomous ODE (17) over the interval Δt with the initial condition $\boldsymbol{q}(t_i) = \boldsymbol{q}_i$

$$\boldsymbol{q}_{i+1} = \boldsymbol{P}_i \cdot \boldsymbol{q}_i + \boldsymbol{S}_i \cdot \boldsymbol{q}_{i-m+1} + \boldsymbol{T}_i \cdot \boldsymbol{q}_{i-m} \tag{18}$$

with

$$\begin{aligned} \boldsymbol{P}_i &= \exp\left(\tilde{\boldsymbol{A}}_i(t_{i+1} - t_i)\right) \in \mathbb{R}^{2n\times 2n}, \\ \boldsymbol{S}_i &= w_\alpha \cdot \boldsymbol{R}_i \in \mathbb{R}^{2n\times 2n}, \end{aligned} \tag{19}$$

$$\begin{aligned} \boldsymbol{T}_i &= w_\beta \cdot \boldsymbol{R}_i \in \mathbb{R}^{2n\times 2n}, \\ \boldsymbol{R}_i &= [\exp(\tilde{\boldsymbol{A}}_i(t_{i+1} - t_i) - \boldsymbol{I}] \cdot \tilde{\boldsymbol{A}}_i^{-1} \cdot \tilde{\boldsymbol{B}}_i. \end{aligned} \tag{20}$$

Defining the state $\boldsymbol{z}$ of a time-discrete system as

$$\boldsymbol{z}_i = [\boldsymbol{q}_i \;\; \boldsymbol{q}_{i-1} \;\; \boldsymbol{q}_{i-2} \;\; \cdots \;\; \boldsymbol{q}_{i-m}]^{\mathrm{T}}, \tag{21}$$

the new state vector can be written as a discrete map, given by

$$\boldsymbol{z}_{i+1} = \boldsymbol{V}_i \cdot \boldsymbol{z}_i \tag{22}$$

with the coefficient matrix

$$\boldsymbol{V}_i = \begin{bmatrix} \boldsymbol{P}_i^{(2n,2n)} & \boldsymbol{0}^{(2n,2n(m-2))} & \boldsymbol{S}_i^{(2n,2n)} & \boldsymbol{T}_i^{(2n,2n)} \\ & \boldsymbol{I}^{(2mn,2mn)} & & \boldsymbol{0}^{(2n,2n)} \end{bmatrix}. \tag{23}$$

The parentheses indicate the dimensions of the specific matrices, $\boldsymbol{I}$ is the identity matrix. The final transition matrix or monodromy matrix $\boldsymbol{\Phi}$ between two successive periods of the system, i.e., one complete rotation of the workpiece, can now be calculated by multiplication of the local transition matrix for each time increment. Thus,

$$\boldsymbol{\Phi} = \boldsymbol{V}_\tau \cdot \boldsymbol{V}_{\tau-1} \cdot \boldsymbol{V}_{\tau-2} \cdots \boldsymbol{V}_{i+1} \cdot \boldsymbol{V}_i, \qquad \boldsymbol{z}_{i+\tau} = \boldsymbol{\Phi} \cdot \boldsymbol{z}_i. \tag{24}$$

In this way, a finite-dimensional approximation of the transition matrix is constructed. The stability of the time-discrete system can be deduced my means of the largest eigenvalue $\lambda_{\max}$ of the transition matrix $\boldsymbol{\Phi}$. The system is stable when $|\lambda_{\max}| < 1$ and unstable when $|\lambda_{\max}| > 1$. The transition curve or boundary of stability corresponds to $|\lambda_{\max}| = 1$.

Since semi-discretization preserves asymptotic stability of the original system, see Hartung et al. [21], the approximation as a time discrete system can be used to draw approximate stability charts.

4 Implementation

Calculation of the transition matrix $\boldsymbol{\Phi}$ using Eq. (24) involves a high number of matrix multiplications and is thus computationally intensive. Therefore, a good approach to improve the efficiency of the stability analysis is to avoid or reduce the cost for these multiplications.

One interesting thing can be observed looking at Eqs. (1) and (18). From the delay term, only the displacement states are needed. So, taking this into consideration, the transition matrix can be constructed more efficiently. Insperger and Stépán [15] excluded the velocity part of the past states. This greatly reduces the size of the state space vector. As a consequence, the size of the transition matrix will also be reduced from $2n(m + 1)$ to $n(m + 2)$. Further, Henninger et al. [16, 20] kept only a reduced state $\boldsymbol{q}_r \in \mathbb{R}^d$ for the past that consisted of the d displacements at the tool contact point needed to calculate the process force. Thus, the size of the transition matrix can be further reduced to $(2n + md) \times (2n + md)$.

Henninger [20] also introduced a direct method which helps to avoid the matrix multiplications entirely. Following that, the equations for all the time increments of one complete rotation are written in matrix form, giving

$$\boldsymbol{\Phi}_l \cdot \boldsymbol{z}_{i+m} = \boldsymbol{\Phi}_r \cdot \boldsymbol{z}_i, \quad \boldsymbol{\Phi}_l, \boldsymbol{\Phi}_r \in \mathbb{R}^{2n(m+1)\times 2n(m+1)}, \tag{25}$$

where

$$\boldsymbol{\Phi}_l = \begin{bmatrix} \boldsymbol{I} & -\boldsymbol{P}_{i+m-1} & 0 & 0 & \cdots & 0 & 0 & 0 \\ 0 & \boldsymbol{I} & -\boldsymbol{P}_{i+m-2} & 0 & \cdots & 0 & 0 & 0 \\ \vdots & \ddots & \ddots & \ddots & \cdots & \ddots & \ddots & \vdots \\ 0 & 0 & 0 & 0 & \cdots & 0 & \boldsymbol{I} & -\boldsymbol{P}_i \\ 0 & 0 & 0 & 0 & \cdots & 0 & 0 & \boldsymbol{E} \end{bmatrix},$$

$$\boldsymbol{\Phi}_r = \begin{bmatrix} \boldsymbol{S}_{i+m-1} & \boldsymbol{T}_{i+m-1} & 0 & 0 & \cdots & 0 & 0 & 0 \\ 0 & \boldsymbol{S}_{i+m-2} & \boldsymbol{T}_{i+m-2} & 0 & \cdots & 0 & 0 & 0 \\ \vdots & \ddots & \ddots & \ddots & \cdots & \ddots & \ddots & \vdots \\ 0 & 0 & 0 & 0 & \cdots & 0 & \boldsymbol{S}_i & \boldsymbol{T}_i \\ 0 & 0 & 0 & 0 & \cdots & 0 & 0 & \boldsymbol{I} \end{bmatrix}. \tag{26}$$

In order to calculate the largest eigenvalue of the transition matrix $\boldsymbol{\Phi} = \boldsymbol{\Phi}_l^{-1} \cdot \boldsymbol{\Phi}_r$, the eigenvalue problem needs to be solved. To avoid the costly calculation of the inverse, the equivalent generalized eigenvalue problem

$$(\boldsymbol{\Phi}_r - \lambda \boldsymbol{\Phi}_l) \cdot \boldsymbol{U} = \boldsymbol{0} \tag{27}$$

is considered. The largest eigenvalue of Eq. (27) can be efficiently determined using the eigs function that is readily available in MATLAB.

For the considered case the direct construction of the transition matrix and solving Eq. (27) is much faster than the successive multiplication using Eq. (24). The direct method will therefore be used in the following investigations.

It is noticed that, though the direct method reduces arithmetic operations, it takes significant time to build the transition matrices $\boldsymbol{\Phi}_l$ and $\boldsymbol{\Phi}_r$ step by step from the $\boldsymbol{P}_i$, $\boldsymbol{S}_i$ and $\boldsymbol{T}_i$. Repeated indexing into the large sparse matrices is slow in MATLAB, even when enough memory has been preallocated. To avoid that, a different approach is applied that builds the transition matrices in one step from three vectors $\boldsymbol{p}_{\text{col}}$, $\boldsymbol{p}_{\text{row}}$ and $\boldsymbol{v}$. The entries $\boldsymbol{p}_{\text{col},i}$ and $\boldsymbol{p}_{\text{row},i}$ of the index vectors $\boldsymbol{p}_{\text{col}}$ and $\boldsymbol{p}_{\text{row}}$ indicate hereby the column and row index of a given entry $\boldsymbol{v}_i$ of the value vector $\boldsymbol{v}$ in the sparse matrix to be build.

Algorithm 1 outlines the procedure to construct the index and value vectors for $\boldsymbol{\Phi}_r$ using pseudocode. For each time increment, matrices $\boldsymbol{S}_i$ and $\boldsymbol{T}_i$ are constructed and then decomposed into local index and value vectors using the ***find*** command. The position in the global matrix of the local values is then calculated by adding an offset to the local row and column position. The so-obtained index and value vectors are a part of $\boldsymbol{p}_{\text{col}}$, $\boldsymbol{p}_{\text{row}}$ and $\boldsymbol{v}$ and stored as a three column matrix $\boldsymbol{z}_i$ in a cell array. After completion of the loop, the ***cell2mat*** is used to assemble a matrix $\boldsymbol{Z}$ from the $\boldsymbol{z}_i$. The transition matrix is then build in one step from the columns of $\boldsymbol{Z}$, which are the global index and value vectors.

Constructing the transition matrices $\boldsymbol{\Phi}_l$ and $\boldsymbol{\Phi}_r$ following the above approach, reduces the computation time significantly. In the examples given in the following section, the computation time could be reduced by a factor of 100 compared to the approach using sparse indexing.

The semi-discretization method preserves asymptotic stability of the continuous system. With increasing number m of discretization intervals, the largest eigenvalue $\lambda_{\max}$ of the time-discrete system will converge towards λ_∞, the true value of the largest eigenvalue of the infinite-dimensional transition matrix of the original system. On the one hand, we need m large enough to ensure that $\lambda_{\max} \approx \lambda_\infty$, and on the other hand, we want m to be small to reduce the computational cost.

Algorithm 1: Compute $\boldsymbol{\Phi}_r$

Require: m, n

Output: $\boldsymbol{\Phi}_r$

$a \leftarrow m$

$y \leftarrow 2 * n * (m + 1)$

for $i := 1$ **to** m **do**

$\boldsymbol{S}_i, \boldsymbol{T}_i \leftarrow \boldsymbol{calculateST}(i)$

$[\boldsymbol{g}, \boldsymbol{h}, \boldsymbol{k}] \leftarrow \boldsymbol{find}\ [\boldsymbol{S}_i\ \ \boldsymbol{T}_i]$ % returns the nonzero entries $\boldsymbol{k}$, and local row and column indices $\boldsymbol{g}$ and $\boldsymbol{h}$

$\{\boldsymbol{r}\} \leftarrow \{\boldsymbol{g}\} + (a-1) * 2 * n$ % calculate the row position in the global matrix

$\{\boldsymbol{u}\} \leftarrow \{\boldsymbol{h}\} + (a-1) * 2 * n$ % calculate the column position in the global matrix

$[\boldsymbol{z}] \leftarrow [\boldsymbol{r}, \boldsymbol{u}, \boldsymbol{w}]$; % store the three vectors into a matrix with 3 columns

$\boldsymbol{Y}\{a, 1\} \leftarrow [\boldsymbol{z}]$ % store the $\boldsymbol{z}$ matrix in the cell $\boldsymbol{Y}$ where cell row "a" will vary at each loop

$a \leftarrow a - 1$

end for

$[\boldsymbol{Z}] \leftarrow \boldsymbol{cell2mat}\{\boldsymbol{Y}\}$ % it converts "$\boldsymbol{Y}$" cell in "$\boldsymbol{Z}$" matrix format

$\boldsymbol{\Phi}_r \leftarrow \boldsymbol{sparse}(\boldsymbol{Z}(:,1), \boldsymbol{Z}(:,2), \boldsymbol{Z}(:,3), y, y, 4 * n * y)$

$\boldsymbol{\Phi}_r(m * n + 1 : y, m * n + 1 : y) \leftarrow \boldsymbol{E}$

Here, an efficient method is used to search the suitable discretization parameter to obtain the satisfactory stability chart of the workpiece models. For quantitative assessment of the convergence behavior, the error rate of the eigenvalue value with respect to the reference eigenvalue λ_∞ is computed for an increasing number of discretization points

$$\epsilon_r = \lg \frac{\lambda(m) - \lambda_\infty}{\lambda_\infty}. \tag{28}$$

From a practical point of view, it is not possible to implement that. So, the eigenvalue $\widetilde{\lambda}_\infty$ for a comparatively large number of discretization points m is set as the reference instead of the true eigenvalue λ_∞.

5 Numerical results and discussion

The semi-discretization method is now implemented to study the stability of the turning of thin-walled cylindrical workpieces. To get a clearer idea about the effect of the workpiece thickness on its dynamic stability, two workpiece models of different thickness are chosen for the analysis. It is considered that the single point cutting tool with carbide cutting tip is used in turning. The cutting tool geometry following standard nomenclature according to the DIN standard 4 971 are $\gamma = 6°$, $\alpha = 5°$, $\lambda = 0°$, $\kappa = 70°$, $\epsilon = 90°$, and $r = 0.8$ mm.

The workpiece material is steel (E295GC). The thicknesses of the models are 6 mm and 3 mm which are referred to as model 1 and model 2. The length of the workpiece has a length of 0.2 m and an inner diameter of 0.06 m. The workpiece is clamped in a three jaw chuck, each jaw is 20 mm wide and 10 mm high. To study the effect of the tool positioning with respect to the jaw on the stability chart, the analysis is done for three different tool positions, 0.2 m, 0.15 m, and 0.05 m.

The Finite Element Model (FEM) of the workpiece consists of 3 280 nodes and 3 200 elements. It was obtained using the Shell 181 element in ANSYS. The mass and stiffness matrices of the FE model are extracted and used to build the system equations in state space form. A model order reduction using the first five modes of vibration is done to reduce the size of the transition matrix as well as the overall computation time. As chatter happens in the vicinity of one of the first eigenmodes, adding higher modes did not contribute in a significant way. A light modal damping of 0.02 is considered.

The general formulation is made for three dimensional cutting forces. The coefficients for the three dimensional cutting force law given by Eqs. (4)–(6) are taken from Paucksch et al. [19]. The specific thrust, cutting and feed forces are thus $K_{t1.1} = 274\,\mathrm{N/mm^2}$, $K_{c1.1} = 1\,500\,\mathrm{N/mm^2}$ and $K_{f1.1} = 351\,\mathrm{N/mm^2}$. The exponents were determined to $m_x = 0.5$, $m_y = 0.29$ and $m_z = 0.7$.

As we know that the cutting force parameters are dependent on the process parameters tool feed and depth of cut, there are two options to draw the stability plot. First, the longitudinal tool feed f can be fixed and the tool depth of cut a_p varied with the rotational speed N. Second, the tool depth of cut can be fixed and the longitudinal tool feed varied. In all cases, the rotational speed range is kept between $600\,\mathrm{min^{-1}}$ and $1\,000\,\mathrm{min^{-1}}$. It should be noted that higher rotational speeds are not feasible due to cutting speed limitations of the equipment.

The convergence of λ_{max} towards $\widetilde{\lambda}_\infty$ is evaluated for six different combinations of speed and feed (or depth of cut) for stable and unstable configurations. Convergence is analyzed separately for all workpiece models and all four positions of the tool. As expected, it is found that the error decreases with the number of discretization intervals. It is interesting to note that the same m leads to different accuracies for different rotational velocities. Consequently, it is concluded that fixing Δt seems to be the best way to ensure the same accuracy independently of the rotational velocity. Note that by doing so, the number of discretization intervals and thus the cost of computation decreases with increasing rotational velocity.

The convergence of the algorithm is analyzed for all three workpiece models and different tool positions. The parameter Δt is then determined such that $\epsilon_r \leqslant 10^{-2}$. For model 1, it was found that a discrete time step of 3.6×10^{-5} ensures the desired accuracy. For models 2 and 3, the step size was 6.4×10^{-5} and 5.7×10^{-5}. It was also found that the time step varies only slightly with the tool position.

The presented stability analysis procedure allows only to deduce stability of one given system. The domain of stable cutting is thus implicitly defined. Inumerable system configurations need to be analyzed in order to determine the domain of stable operation. To limit the number of tested system configurations, an adaptive mesh refinement is used to obtain the boundary of stability.

Figures 7 and 8 show the stability charts for model 1

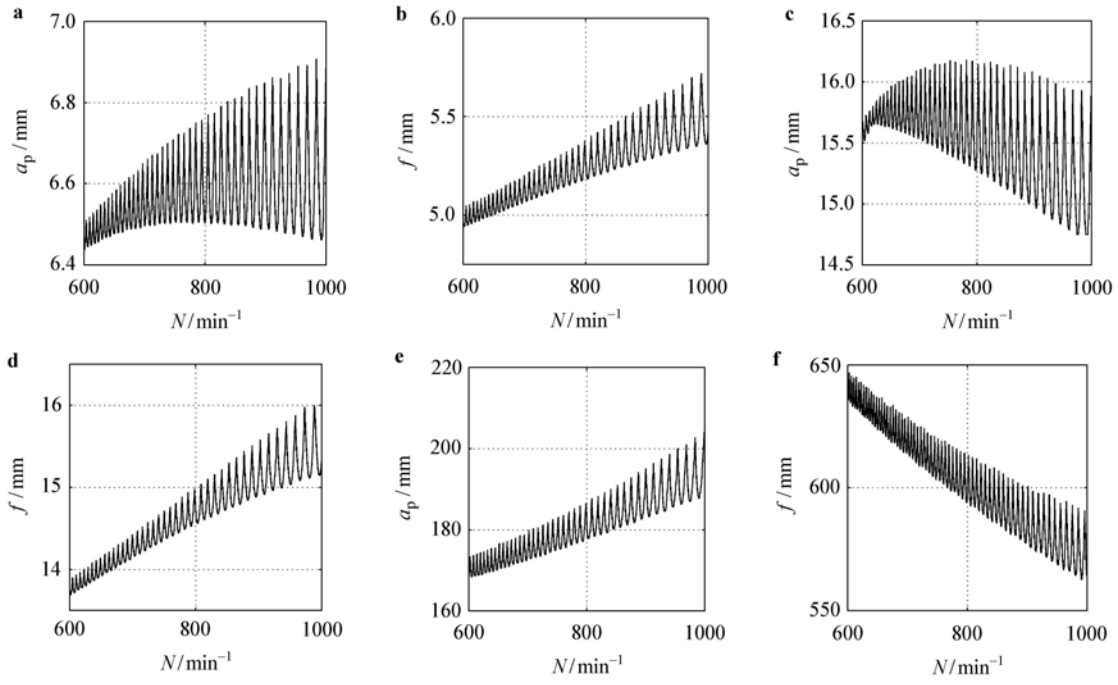

Fig. 7 Stability charts for model 1 with varying depth of cut and varying feed. **a** Fixed feed, position 0.2 mm; **b** Fixed depth of cut, position 0.2 mm; **c** Fixed feed, position 0.15 mm; **d** Fixed depth of cut, position 0.15 mm; **e** Fixed feed, position 0.05 mm; **f** Fixed depth of cut, position 0.05 mm

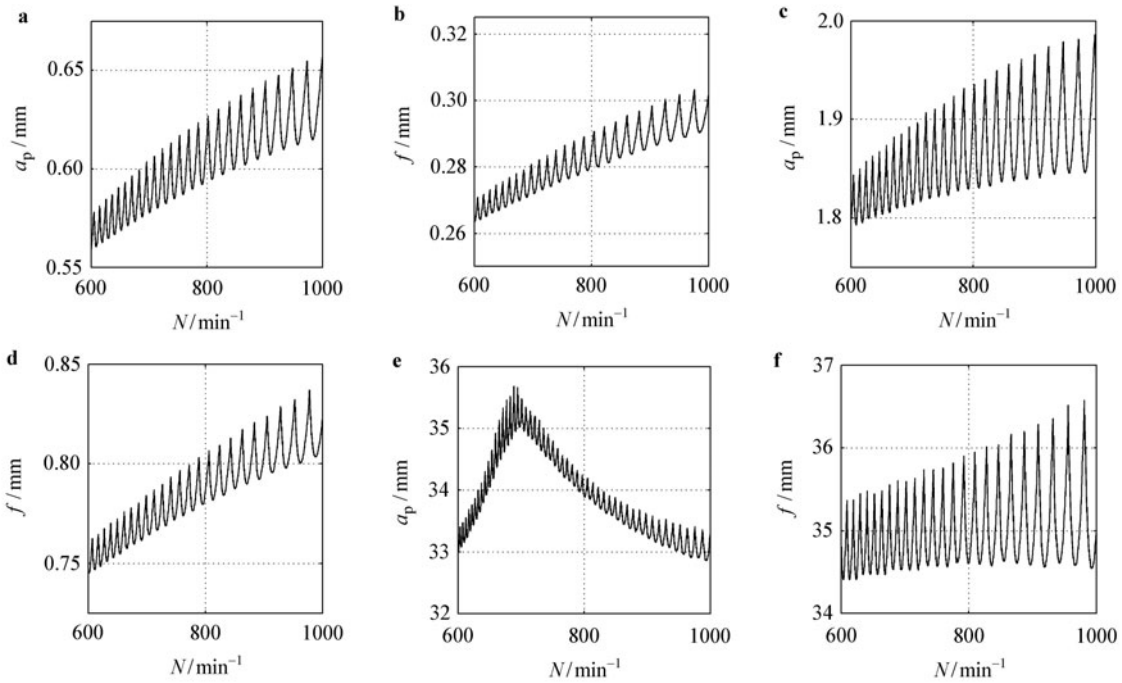

Fig. 8 Stability charts for model 2 with varying depth of cut and varying feed. **a** Fixed feed, position 0.2 mm; **b** Fixed depth of cut, position 0.2 mm; **c** Fixed feed, position 0.15 mm; **d** Fixed depth of cut, position 0.15 mm; **e** Fixed feed, position 0.05 mm; **f** Fixed depth of cut, position 0.05 mm

and model 2. The charts have been obtained for either a fixed feed per rotation of $f = 0.1$ mm or a fixed depth of cut of $a_p = 0.1$ mm. The boundary of stability is then parametrized using the rotational velocity and depth of cut or feed. It should be noted that model 1 will not become unstable under the assumptions made in this work using feasible process parameters, i.e., a depth of cut below 6 mm and a feed below 2 mm per rotation. The interest, however, is to observe the influence of different parameters on the stability.

From the stability charts of model 1 and model 2, it may be said that the domain of stable operation is the largest when the tool is close to the jaw end. For realistic process parameters, no unstable machinig would occur this close to the jaw. Machining is therefore most critical when the process starts, e.g., when the tool is farthest from the jaw. As machining progresses, the parameters could therefore be modified to reduce cycle time, e.g., by increasing the feed.

Interesting is the influence of the spindle speed. Stability charts for different tool positions exhibit different characteristics. For model 1 and fixed feed, with the increase of speed, the stability starts to increase initially and then decreases when the tool position is at 0.2 m and 0.15 m. When the tool is at 0.1 m, the stability decreases sharply with the increase of rotational speed. When the tool position is at 0.05 m, close to the jaw, stability increases with the increase of speed. For fixed depth of cut, with the increase of speed, the stability boundary increases when the tool position is 0.2 m, 0.15 m, and 0.1 m. When the tool is at 0.05 m, the stability boundary goes down sharply. For model 2, i.e., lower wall thicknesses, an increase of rotational speed seems to slightly increase stability.

6 Conclusions

From the implementation point of view, the semi-discretization method is successfully applied to analyze stability of the time-variant periodic turning operation for thin-walled cylinder. The successive method and the direct method: Two different ways to construct the transition matrix of the system are available. But, as the successive method multiplies a number of local transition matrices, it does not reduce computation time that much in spite of the reduced past state vector.

On the other hand, the size of the obtained matrix is larger using the direct method, as the state vector can not be reduced for past states. But, the final transition matrix is generated at once. Hence, the computational cost for the matrix multiplication in the direct method is avoided. Therefore, finally, the direct method, used by Henninger and Eberhard [20], is adopted to generate the transition matrix in this semi-discretization method. To constitute the transition matrix, a different approach is implemented in MATLAB code which reduces the computation time significantly.

The mass and stiffness matrices, obtained from ANSYS are used to present the thin walled turning operation as a time variant periodic delay system in state space form. The three dimensional cutting force vector is also incorporated in the system equation. Before stability charts were drawn, the precision of the eigenvalue calculation is analyzed for different

system configurations and system discretization. In order to have results of similar quality throughout the chart, the size of the discretization intervals instead of the number of intervals is chosen as parameter. Stability charts for two different workpiece models and three different tool positions are then calculated. Form the stability charts, it can be concluded that the zone of stable cutting increases when the tool comes closer to the jaw end.

It is very interesting to see that the stability boundary sometimes increases or decreases with increasing rotational speed, depending on the thickness of the workpiece model and the position of the tool. However, the machining is stable when the fixed parameter, i.e., feed or depth of cut, is lowered. So, it may be concluded that the ratio of the longitudinal feed and depth of cut of the tool can be controlled to obtain stable turning.

Acknowledgement This research work was partially done while Arnab Chanda visited the University of Stuttgart from September 2010 to May 2011 under DAAD-IIT Sandwich Master Program funded by a DAAD M.Sc. Scholarship. The doctoral research of Achim Fischer was funded since 2010 by the Baden-Württemberg Stiftung and the Stuttgart Cluster of Excellence Simtech. The research work and some of the underlying codes started in the doctoral thesis research of Christoph Henninger at the ITM, University of Stuttgart. All this support and help is greatly appreciated.

References

1 Taylor, F.: On the art of cutting metals. Transactions of the ASME **28**, 31–350 (1907)
2 Arnold, R.: The mechanism of tool vibration in the cutting of steel. Proceedings of the Institution of Mechanical Engineers **154**, 261–284 (1946)
3 Tobias, S.A.: Machine-Tool Vibration. Blackie and Sons, London (1965)
4 Merrit, H.E.: Theory of self-excited machine-tool chatter. Journal of Engineering for Industry **87**, 447–454 (1965)
5 Tlusty, J., Polacek, M.: The stability of machine tools against self-excited vibrations in machining. ASME International Research in Production Engineering **1**, 465–474 (1963)
6 Clancy, B.E., Shin, Y.C.: A comprehensive chatter prediction model for face turning operation including tool wear effect. International Journal of Machine Tools and Manufacture **42**, 1035–1044 (2002)
7 Ozlu, E., Budak, E.: Analytical modeling of chatter stability in turning and boring operations. Part I: Model development. Journal of Manufacturing Science and Engineering **129**, 726–732 (2007)
8 Ozlu, E., Budak, E.: Comparison of one-dimensional and multi-dimensional models in stability analysis of turning operations. International Journal of Machine Tools and Manufacture **49**, 1042–1047 (2009)
9 Li, Z.Q., Liu, Q.: Solution and analysis of chatter stability for end milling in the time-domain. Chinese Journal of Aeronautics **21**, 169–178 (2008)
10 Srinivas, J., Kotaiah, K.: A study of bifurcation behaviour in oblique turning operation. International Journal of Machine Tools and Manufacture **49**, 1042–1047 (2009)
11 Mehdi, K., Rigal, J., Play, D.: Dynamic behavior, thin walled cylindrical workpiece during the turning process. Part 2: Cutting process simulation. Transactions of ASME, Journal of Manufacturing Science and Engineering **124**, 532–568 (2002)
12 Mehdi, K., Rigal, J., Play, D.: Dynamic behavior, thin walled cylindrical workpiece during the turning process. Part 2: Experimental approach and validation. Transactions of ASME, Journal of Manufacturing Science and Engineering **124**, 569–580 (2002)
13 Bayly, L.K., Davis, M.A.: Stability of interrupted cutting by temporal finite element analysis. Journal of Manufacturing Science and Engineering **125**, 220–225 (2003)
14 Insperger, T., Stépán, G.: Semi-discretization method for delayed systems. International Journal for Numerical Methods in Engineering **55**, 503–518 (2002)
15 Insperger, T., Stépán, G.: Updated semi-discretization method for periodic delay-differential equations with discrete delay. International Journal for Numerical Methods in Engineering **61**, 117–141 (2004)
16 Henninger, C., Eberhard, P.: Improving the computational efficiency and the accuracy of the semi-discretization method for periodic delay-differential equations. European Journal of Mechanics A/Solids **27**, 975–985 (2008)
17 Gawronski, W.K.: Advanced Structural Dynamics and Active Control of Structures. Springer, New York (2004)
18 König, K., Essel, W., Witte, L.: Spezifische Schnittkraftwerte für die Zerspanung metallischer Werkstoffe. Verein Deutscher Eisenhüttenleute. Verlag Stahleisen mbH, Düsseldorf (1982) (in German)
19 Paucksch, E., Holsten, S., Linß, M., et al.: Zerspantechnik. Vieweg+Teubner, Wiesbaden (2008) (in German)
20 Henninger, C.: Methoden zur simulationsbasierten Analyse der dynamischen Stabilität von Frässprozessen, doctoral thesis, Schriften aus dem Institut für Technische und Numerische Mechanik der Universität Stuttgart, Shaker Verlag, Aachen (2009) (in German)
21 Hartung, F., Insperger, T., Stépán, G., et al.: Approximate stability charts for milling processes using semi-discretization. Applied Mathematics and Computation **174**, 51–73 (2006)
22 Hale, J.K., Lunel, S.M.V.: Introduction to Functional Differential Equations. Springer, New York (1993)